Available online at www.sciencedirect.com
SCIENCE DIRECT®
Physics of the Earth and Planetary Interiors 155 (2006) 260–268
PHYSICS OF THE EARTH AND PLANETARY INTERIORS
www.elsevier.com/locate/pepi

Phase stability of $CaSiO_3$ perovskite at high pressure and temperature: Insights from ab initio molecular dynamics

Li Li [a,b,*], Donald J. Weidner [a,b], John Brodholt [a], Dario Alfè [a], G. David Price [a], Razvan Caracas [c], Renata Wentzcovitch [c]

[a] *Department of Earth Sciences, University College London, Gower Street, London WC1E6BT, UK*
[b] *Mineral Physics Institute, Department of Geosciences, University of New York at Stony Brook, Stony Brook, NY 11790, USA*
[c] *Department of Chemical Engineering and Material Science, Minnesota Supercomputing Institute, University of Minnesota, Minneapolis, MN 55455, USA*

Received 7 September 2005; received in revised form 2 December 2005; accepted 20 December 2005

Abstract

We report the dynamics of the structure of $CaSiO_3$ perovskite from ab initio molecular dynamics (AIMD) calculations at high pressure (P up to 130 GPa) and high temperature (T up to 5000 K). Our calculations indicate three separate stability fields: orthorhombic, tetragonal and cubic, with the tetragonal phase dominating the pressure and temperature region between room temperature and 4000 K. These regions are defined by the stress symmetry of the AIMD calculation. The boundary between the orthorhombic and the tetragonal structures is found to have a positive Clapyron slope and is close to room temperature at low pressure. The boundary is marked by the transition from stable, constant octahedral tilts, to dynamically varying tilts that change sign with time. The calculated atom positions indicate that the orientation of the octahedra can be noted as $a^-a^-c^+$ in the orthorhombic phase ($T = 150$ K). The magnitude of the octahedra rotation varies little over the entire P–T range at high T (1000 K and above) while, at elevated temperature, the rotation angles of the octahedra oscillate positively and negatively with time. The tetragonal structure is probably due to a shortened Si—O bond distance along one axis. Calculated X-ray diffraction patterns indicate small super-lattice reflections that could result from the octahedral rotations throughout the P, T region investigated. The small spontaneous strain of the tetragonal phase relative to the aristotype, cubic phase, throughout conditions appropriate to the lower mantle, creates the possibility for seismic energy absorption (low Q) in the deep Earth.

Keywords: $CaSiO_3$ perovskite; Phase stability; Dynamic structure; Lower mantle

1. Introduction

During the last several years, consensus has been growing that $CaSiO_3$ perovskite is not stable in the cubic form at high pressure (Adams, 2004; Akber-Knutson et al., 2002; Caracas and Wentzcovitch, 2005; Jung and Oganov, 2005; Magyari-Kope et al., 2002; Ono et al., 2004; Shim et al., 2002; Wentzcovitch et al., 1995). Ferroelastic phase transitions in materials such as $CaSiO_3$ perovskite are challenging to identify experimentally and theoretically. Close to the transition boundary with increasing symmetry, X-ray diffraction peaks, that were once separate, merge, and small super-lattice diffraction peaks disappear. Thus, it becomes difficult to clearly

* Corresponding author.
E-mail address: lilli@ic.sunysb.edu (L. Li).

0031-9201/$ – see front matter © 2006 Elsevier B.V. All rights reserved.
doi:10.1016/j.pepi.2005.12.007

define the phase of a solid close to the boundary with such tools. Theoretically, the different polymorphs have very similar energies, making it difficult to define the stable phase. Recent progresses in both the theoretical and experimental studies of $CaSiO_3$ perovskite are due to the improvements in the methods used.

While the different polymorphs of perovskite are crystallographically very similar, they can have quite different properties (Carpenter et al., 2000). Furthermore, being close to the phase boundary can introduce new phenomena, such as soft vibrational modes, which can cause some shear velocity to become very low or even to vanish (Carpenter et al., 2000), or high attenuation of acoustic waves as domain wall boundaries become very mobile (Harrison et al., 2003). Both of these effects could produce significant signals on the seismic record. $MgSiO_3$, perovskite has been shown to be far from a ferroelastic phase transformation by both theory and experiments (Karki et al., 2001; Oganov et al., 2001; Shim et al., 2001; Stixrude and Cohen, 1993; Wentzcovitch et al., 1995; Wolf and Jeanloz, 1985). Thus, the primary candidate for a deep earth ferroelastic phase transition is $CaSiO_3$ perovskite. Here we present the results of an ab initio high temperature study of the stable distortions of this phase using molecular dynamics. We conclude that the cubic phase is not entirely stabilized even at temperatures of the Earth's lower mantle. While we find that the elastic moduli are not appreciably softened (Li et al., 2005), the attenuation due to the ferroelastic character of $CaSiO_3$ perovskite may make this phase very distinctive in its seismic signature.

2. Computational method

Ab initio molecular dynamics (AIMD) simulations were performed to calculate the state properties of $CaSiO_3$ perovskite using VASP code (Kresse and Furthmüller, 1996a,b). The exchange-correlation functional E_{xc} is the PW91 form of the generalized gradient approximation (GGA) (Perdew et al., 1992; Wang and Perdew, 1991). We use projector-augmented-wave (PAW) implementation of density functional theory (DFT) and the implementation of an efficient extrapolation for the charge density (Alfè, 1999; Blöchl, 1994; Kresse and Joubert, 1999). All calculations were performed using an 80-atom super-cell. A plane-wave cutoff energy 500 eV was shown to be sufficient for the structures to converge. Γ point was used for sampling the Brillouin zone. The time step used in the dynamical simulation was 1 fs. The core radii are 2.3 a.u. for Ca (core configuration $1s^2\ 2s^2\ 2p^6$), 1.9 a.u. for Si ($1s^2\ 2s^2\ 2p^6$) and 1.52 a.u. for O ($1s^2$).

The unit cell of the perovskite for most of these calculations was oriented with one axis parallel to the pseudo-cubic axis and the other two axes rotated 45° from the pseudo-cubic axes. Cell lengths of the three axes thus become $\sqrt{2}a$, $\sqrt{2}a$, a, where a is the cubic cell length. The molecular dynamics box is then $2 \times 2 \times 2$ of these unit cells containing 80 atoms. This orientation was chosen to allow maximal freedom of the unit cell to distort from its cubic form to *Pbnm*, the stable form of the analogue, $MgSiO_3$ perovskite. The stresses for a cubic box were calculated over at least 2 ps of simulation. Tests showed that longer simulation has little effect on the calculated results. Error analysis for the stresses are performed following the algorithm described by Allen and Tildesley (1997). The first criterion for being a stable cubic phase is whether the stresses on the 80 atom box is hydrostatic or not. If not, then the dimensions of the cell were modified until the stress became hydrostatic.

3. Phase stability

Fig. 1 illustrates the phase diagram for $CaSiO_3$ perovskite based on the stress analysis of the 80 atom box whose initial dimensions were $2\sqrt{2}a$, $2\sqrt{2}a$, $2a$. The labels of cubic, tetragonal, and orthorhombic are simply based on the cell dimension of the hydrostatic equilibrated structure. The principle stresses for the cubic box are illustrated in Fig. 2 as a function of pressure and temperature. In this setting, the shear stresses are all zero for all of the phases. A systematic stress difference of magnitude between 1 and 5 GPa of the c axis relative to the a and b axes persists over a wide pressure and temperature range. When the differences fall beneath the uncertainty

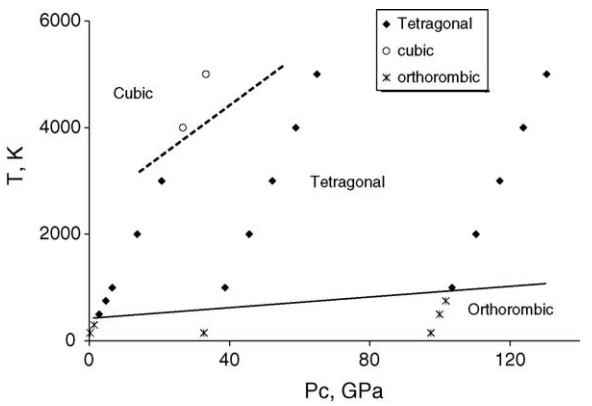

Fig. 1. Calculated phase diagram of $CaSiO_3$ perovskite. Below the solid line, an orthorhombic phase is stable; above the dashed line, a cubic phase is stable. The tetragonal phase that dominates the plot is tetragonal on an instantaneous time scale (1 fs), but probably "cubic" when averaged over time (1 ps).

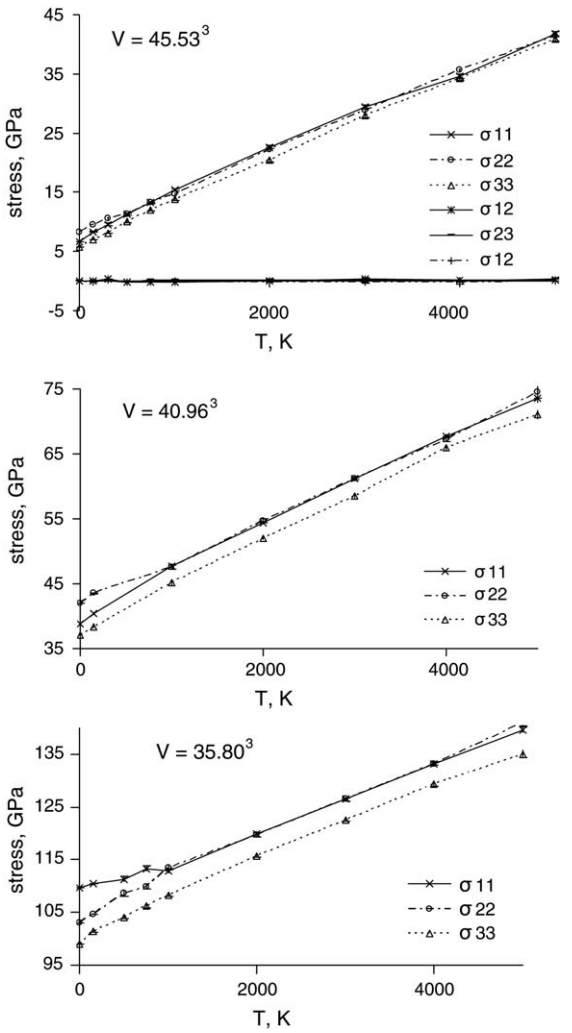

Fig. 2. Calculated stress σ_{11}, σ_{22} and σ_{33} vs. temperature (T) for cells with $a=2\sqrt{2}d_0$, $b=2\sqrt{2}d_0$ and $c=2d_0$ at three volumes (V) (d_0 is the size of a cubic unit cell) and $T=0$–5000 K. σ_{12}, σ_{23} and σ_{13} are close to zero in all cases, thus only shown in $V=45.53$ Å^3. In general, σ_{33} is lower than both $\sigma_{11}$and σ_{22} except $V=45.54$ Å^3 and $T=5000$ K. The difference between $\sigma_{11}$and σ_{22} varies with T. At $V=45.53$ Å^3, calculations were performed at 0, 150, 300, 500, 750 K and higher. $(\sigma_{11}-\sigma_{22})/\sigma_{11}$ is about 10% when $T<500$K. At $T\geq 500$K, $\sigma_{11}=\sigma_{22}$ within the resolution. At $V=35.80$ Å^3, calculations were performed at 0, 150, 500, 750, 1000 K and higher. The difference between σ_{11} and σ_{22} is about 3% when $T<1000$ K. At $T\geq 1000$ K, $(\sigma_{11}-\sigma_{22})/\sigma_{11}<0.5\%$. AIMD calculations were performed to derive a cell in hydrostatic condition by optimising the cell parameters. The hydrostatic cell parameters show the following relationship: $a=b>c$ at $T>1000$ K for the cells with three V. These results suggest that $CaSiO_3$ perovskite experience a second-order phase transition from orthorhombic to tetragonal. At low pressure (~10 GPa), this phase transition occurs between 300 and 500 K; at high pressure (~120 GPa), this phase transition occurs between 750 and 1000 K. A higher transition temperature at higher pressure for $CaSiO_3$ perovskite indicates a exothermic phase boundary. Cubic structure was found only at $V=45.53$ Å^3 and $T>4000$ K.

Table 1
Unit cell dimensions for the tetragonal phase

P (GPa)	T (K)	a (Å)	b (Å)	c (Å)	$1-c/a$	V (Å^3)
6.6	1000	3.5785	3.5785	3.5556	0.0064	45.53
13.7	2000	3.5827	3.5827	3.5472	0.0099	45.53
20.7	3000	3.5811	3.5811	3.5506	0.0085	45.53
38.6	1000	3.4640	3.4364	3.4064	0.0166	40.55
45.4	2000	3.4541	3.4541	3.4332	0.0064	40.96
52.0	3000	3.4515	3.4515	3.4384	0.0038	40.96
58.6	4000	3.4563	3.4563	3.4288	0.0080	40.96
103.4	1000	3.3040	3.3040	3.2796	0.0074	35.80
110.5	2000	3.3028	3.3028	3.2821	0.0099	35.80
117.5	3000	3.3029	3.3029	3.2817	0.0050	35.80
123.7	4000	3.3047	3.3047	3.2781	0.0070	35.80

level, as it does at the highest temperature for the largest volume, then the phase is defined as cubic. Throughout the 'tetragonal' field, the non-hydrostatic stress is an order of magnitude greater than the uncertainty arising from the time-step to time-step variation. It thus appears that a tetragonal phase is stable over the major region of the Earth's lower mantle.

An orthorhombic phase (all principle stresses are different) is stable at lower temperature. A Clapyron slope of about 5 K/GPa separates the orthorhombic phase from the tetragonal phase. At high pressure, the orthorhombic phase is the stable room temperature phase, while at low pressure the tetragonal field covers room temperature.

Table 1 gives the cell dimensions of the tetragonal phases as a function of P and T. These dimensions are determined by varying the cell shape until the calculated stress is hydrostatic within the uncertainty of the calculation. The values are given relative to the pseudo-cubic cell for a primitive cell along with the axis ratios. Table 2 gives similar values for the orthorhombic phase where the results are presented for the rotated coordinate system. The tetragonal phase is characterized by $c<a$; the distortion from cubic $(1-c/a)$ span from 0.6% to 1.0%. The calculated distortions in the orthorhombic phase are about 0.8% for $(1-b/a)$ and 1.5% for $(1-c/a)$. Our calculated results are in agreement with the experimental results of Shim et al. (2002) who used monochromatic X-rays at pressures between 20 and 50 GPa and room temperature after quenching from higher temperatures, find evidence for a tetragonal phase with $c<a$ with the distortion in the range of 0.4–0.7%. The model for the tetragonal phase, as with the experimental observations does not indicate a marked change in distortion with pressure. The consistency of the experiments and theory indicates that the tetragonal phase is the stable room pressure phase over this pressure range and, therefore, the orthorhombic phase is stable at lower temperatures.

Table 2
Unit cell dimensions for the orthorhombic phase

P (GPa)	T (K)	a (Å)	b (Å)	c (Å)	$1-a/b$	$1-a/\sqrt{2}c$	$1-b/\sqrt{2}c$
0.2	150	10.0038	10.0598	7.0180	0.0056	−0.0079	−0.0136
36.4	150	9.7977	9.7195	6.8129	−0.0081	−0.0169	−0.0088
97.2	150	9.4143	9.3121	6.5336	−0.0110	−0.0189	−0.0078

In order to test whether or not the choice of box shape affects the stability of a tetragonal phase, we performed the MD calculations on an 80 atom sample in the aristotype cubic coordinate system of $2a \times 2a \times 4a$ dimension at 2000 K and 50 GPa (the center of the 'tetragonal' field). Indeed, the time average stresses for the cubic box were hydrostatic. However, the time average of the differential stress, $|\sigma_3 - \sigma_1|$ is 4 GPa, about the same value as the time average differential stress deduced in the rotated system. We conclude that on the femto-second time scale for this cubic oriented model, the structure is tetragonal. However, the dynamics associated with the ferroelastic twinning has the effect of interchanging the axes, and makes the time-averaged structure cubic. It seems therefore that the box shape has an influence on the dynamics of the system. Both simulation orientations show that a tetragonal structure is stable on a short time scale, but the rotated coordinate system dynamically stabilizes the tetragonal phase. Which box orientation provides the best approximation to an infinite sized sample is difficult to deduce, but we take the view that both orientations indicate the presence of a tetragonal symmetry, at least on some time scale, and the rotated coordinate system stabilizes this structure. Thus, to examine the properties of this tetragonal phase further, we use the rotated coordinate system for the following studies.

4. Phase characterization

The multiple polymorphs of perovskite are derived from the cubic structure, illustrated in Fig. 3, by a combination of rotations and distortions of the octahedra (Glazer, 1972, 1975). Following Glazer's (1972) notation, we define rotations of the octahedra about the cubic axes a, b, c as α, β, γ. Allowing alternating planes of octahedra to rotate either in phase or out of phase, ridged body rotations of the Si-bearing octahedra can generate 23 distinct crystal structures whose symmetry vary from monoclinic to cubic. The rotations shorten the cell edge lengths as $a = 2d_{\mathrm{Si–O}}\cos(\beta)\cos(\gamma)$, where $d_{\mathrm{Si–O}}$ is the oxygen–silicon distance. We calculate the rotation angles of the structure at each time step by analyzing the displacement of the oxygen perpendicular to the Si–O bond, treating each plane of octahedra separately. This gives 16 independent displacements to define each of the six rotation angles. A sample of the time dependence of these angles is illustrated in Fig. 4 for several temperatures at the largest volume of this study. At the lowest temperature, 150 K, two adjacent planes along the x axis are rotated by about 4°, but in opposite directions. The β angle is also about 4° and is also out of phase for two parallel planes. The γ angle has the same phase for both planes of octahedra along the c axis, with a magnitude of about 2°. In Glazer's (1972) notation, this would be considered an $a^-a^-c^+$ distortion, which yields the *Pbmn* space group, consistent with the orthorhombic dimensions for the hydrostatically stressed cell ($a \neq b \neq c$).

By 300 K, a low frequency vibration allows a couple of short reversals during the 2 ps of time for α, during which β remains stable while γ is now averaging closer to a value of zero. This would be classified as $a^-a^-c^0$, distortion or a *Imcm* space group. By 500K, the long period reversals of the α and β angles, with a period of about 1 ps become dominant, but the normal oscillations of about 150 ps of the octahedra persists throughout the whole temperature range of 150–4000 K illustrated in

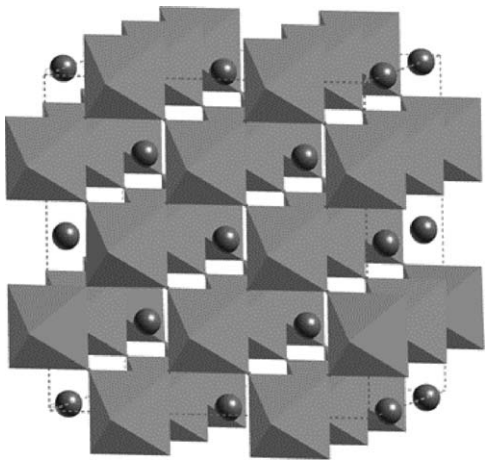

Fig. 3. The perovskite crystal structure. This image represents the 80 atoms that were included in the molecular dynamics calculations. The calcium cation is represented by the sphere, oxygen is located at the corners of the octahedra and silicon is inside the octraheron. Periodic boundary conditions extend the structure in all directions.

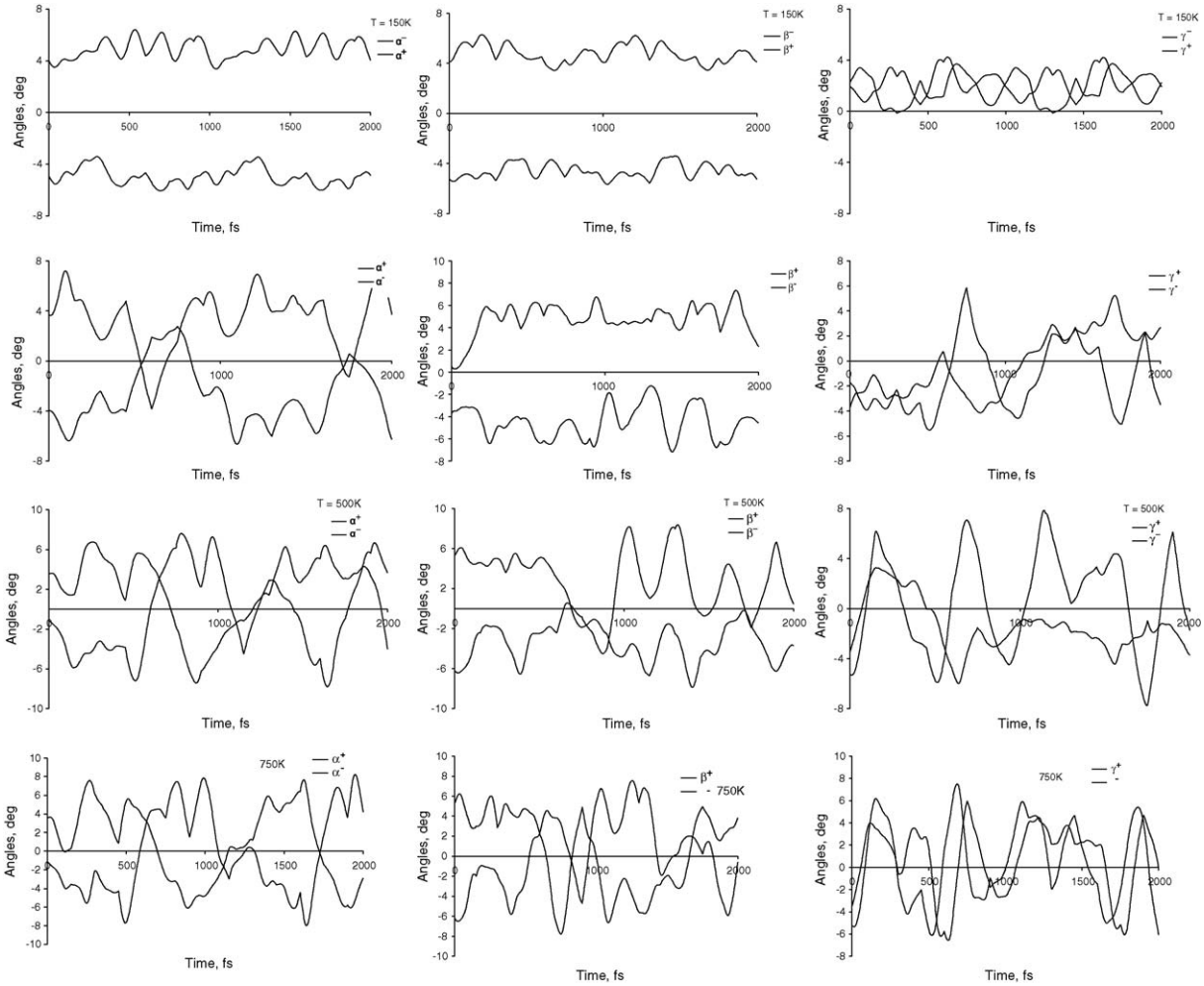

Fig. 4. Calculated octahedral tilt angles (α, β and γ, from left to right) as a function of time at several representative temperatures (150, 300, 500 and 750 K, from top to bottom) for a cell volume of 45.53 Å^3. The solid and broken lines represent the tilts of adjacent planes of octahedra.

this figure. By 500 K the γ angle is oscillating about zero with no apparent phase relationship between the two sets of octahedra. Thus, in the region where a orthorhombic phase transforms to a tetragonal phase ($a = b \neq c$), the octahedra transform from stable $a^-a^-c^+$ configuration to one where the octahedra are oscillating (+) to (−), with a gradual loss of coherence between the adjacent planes with increasing temperature. Fig. 5 illustrates the Si–O

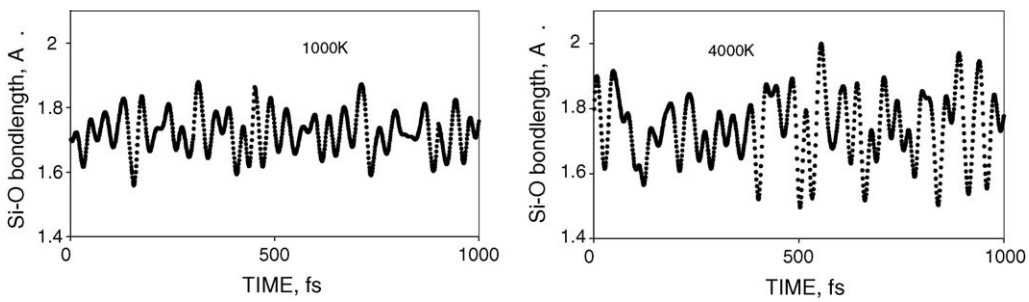

Fig. 5. Si—O bond lengths as a function of time for a cell volume of 45.53 Å^3. The Si—O bond lengths variations increase with temperature while the oscillation period remains fairly constant at about 80 fs.

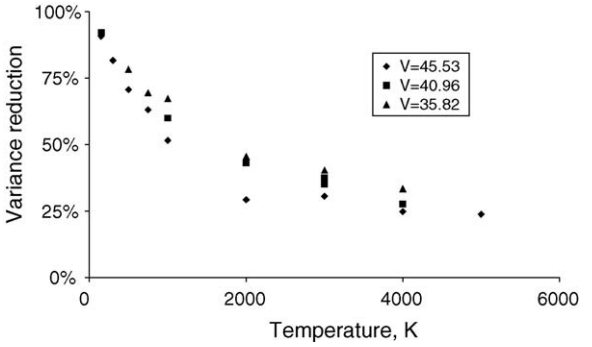

Fig. 6. The variance reduction of the oxygen displacement perpendicular to the Si—O bond due to octahedral tilting. This value decreases with temperature but is reasonably independent of cell volume. The decrease with temperature indicates increasing displacements that distort rather than tilt the octahedra.

bond length as a function of time for a two typical temperatures. The Si–O bond lengths change significantly with temperature, but the frequency is much higher than that of the octahedral rotation, indicating that the calculated octahedral angles are not contaminated with the Si–O interaction. In order to confirm that we see signal in the calculated octahedral rotation, we calculate the variance reduction of the oxygen displacements that are used to calculate the rotations. These are plotted in Fig. 6 as a function of temperature. At low temperature, there is about a 90% reduction in the variance and this reduces to about 30% at the highest temperatures. This suggests that about 70% of the oxygen displacement perpendicular to the Si–O bond distorts the octahedra while 30% is associated with a synchronized rotation of all of the octahedra in any one plane, certainly a strong signal at such high temperatures.

Throughout the broad temperature range, the magnitude of the octahedral rotation and the period remain quite constant. The phase transformation is accompanied by a longer period oscillation – a soft mode – that has sufficient magnitude as to change the sign of the rotation. This mode disappears as the fundamental oscillation of the octahedra has sufficient amplitude to cross the zero line. A value of the octahedral rotation which averages over the six rotation angles and averages over time is illustrated as a function of temperature in Fig. 7. As these rotations indicated no dependence on pressure, we give only one value for each temperature. Indeed, the angles do not vary with temperature either. They remain slightly under four degrees from 150 to 5000 K. That the structure undergoes phase transformations with increasing temperature is more a reflection of the space and time average of the structure, but not the local structure.

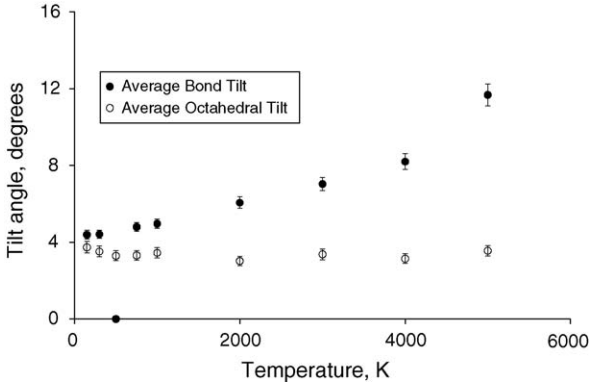

Fig. 7. Octahedral tilt angles as a function of temperature. The open symbols represent the time average of the tilt angle calculated from the octahedral tilts of each frame spaced 1 ps apart and averaged over at least 1000 frames. The closed symbols represent the octahedral tilts that are needed to rationalize the ratio of the average Si—O bond length and the cell edge length. The difference between the two curves must be due to O—Si—O angles that distort the octahedron rather than tilt it.

Fig. 8 illustrates the average Si–O bond length as a function of temperature at constant volume. A zero slope of these lines would be consistent with the quasi-harmonic approximation. While all of the points tend to indicate a slight increase of the Si–O distance with temperature, the greatest departure from constancy is at the lowest pressure and highest temperature, where the anharmonic contributions are expected to become significant. The 4000 and 5000 K points at the largest volume are the conditions where the hydrostatic cell was cubic within the uncertainty of the calculation, which may also be related to the change in character of the Si–O bond here. If the cell volume remains constant and the average Si–O bond increases with temperature, then the Si–O bond-angle distortion from the perfect cubic structure must increase with temperature. Fig. 7,

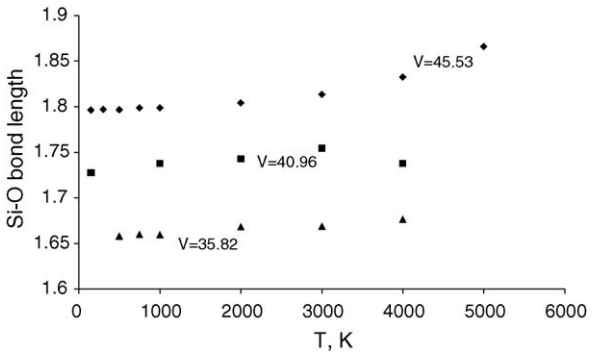

Fig. 8. The time averaged Si—O bond lengths as a function of temperature. Each set of data points correspond to a fixed volume. The departure from a fixed value indicates anharmonic behavior and an increase in value requires increased O—Si—O angles.

depicts this angle as a function of temperature. Here we present the octahedral tilts that are needed to rationalize the ratio of the average Si–O bond length and the cell edge length. As we see, the actual octahedral rotation remains constant with temperature while the distortion angle induced by increasing the Si–O distance is nearly equal to the octahedral rotation angle at low temperature, but nearly triples by 5000 K. The difference between these two angles must be a distortion of the octahedra and is consistent with the observation that the octahedral rotation accounts for only about 1/3 of the angular distortion at these high temperatures.

We can summarize the roles of pressure and temperature on the sample volume as follows. Changes in pressure shorten the Si–O bond but have little effect neither on the octahedral rotations nor on the octahedral distortions. Temperature increases at constant volume causes the average Si–O bond to increase slightly. This increase is accommodated entirely by distortions of the octahedra with no increase in the rotation of the octahedra. This would mean that at constant pressure, temperature increases volume mostly by increasing the Si–O bond. In fact, the Si–O bond increases slightly more than the volume, with compensation coming from the distortion of the octahedra.

Once the rotation angles begin to change sign, then the average structure should become cubic unless the octahedra themselves are distorted. Indeed, the Si–O bond length is shorter in the *c* direction than in the *a–b* plane. Fig. 9 illustrates the average Si–O bond length ratio between that parallel to the *c* direction and that perpendicular to it. This is compared with the tetragonal distortion for the hydrostatic cell, namely the *c/a* ratio of the unit cell. The similarity of these curves implies that the tetragonal distortion is the result of the anisotropy of the Si–O bond length in the octahedron. Perhaps, the orthorhombic setting of the molecular dynamics calculation helped organize the short Si–O bonds, yielding the tetragonal structure in this setting. We expect that indeed, the local structure will be tetragonal, but the short axis might be averaged over time to yield a cubic structure, in much the same manner that the octahedral tilts are averaged in time. Measurements, that are sensitive to local structures (hundreds of atoms) and short time spans, will see a tetragonal or perhaps an orthorhombic structure. Those measurements that average over large volumes or times longer than a pico-second, will sense a cubic structure. In a companion paper (Li et al., 2005), we present the single crystal elastic moduli for $CaSiO_3$ perovskite at these different conditions for all of these structures. We find that, within computational error, the symmetry of the elasticity tensor is consistent with cubic even with the stabilized tetragonal structure. Thus, the material may be close enough to a cubic structure that many of the physical properties will assume a *pseudo-cubic* character.

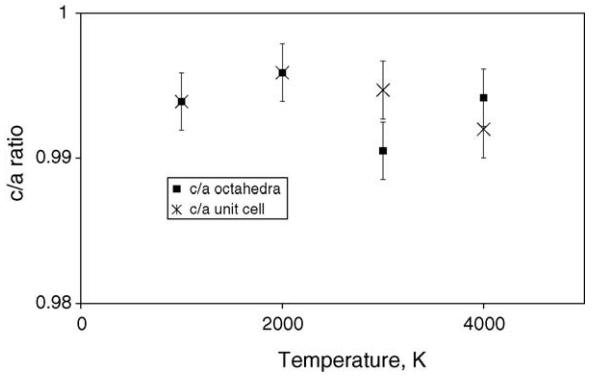

Fig. 9. The *c/a* ratio of the tetragonal cell and of the octahedra. The time averaged Si–O bond lengths parallel to the *c* axis are compared with those perpendicular to the *c* axis. This ratio is then in turn compared to the tetragonal distortion that is necessary to produce a hydrostatic stress field. The values represent an average for the three volumes that have been studied here, as there is no apparent volume dependence of this value. The similarity of these values suggests that the principle cause of the tetragonal distortion is the distortion of the octahedra.

5. Diffraction implications

We calculate the expected X-ray diffraction pattern by determining the structure factor for each femto-second time step, then by adding together the patterns of over 1000 steps. These integrated spectra are calculated for each temperature for the hydrostatic structure. The calculated X-ray diffraction patterns for the largest volume (lowest pressure) system are representative of all of the calculations and are illustrated in Fig. 10. The peaks are identified referenced to the cubic cell. All of the main peaks, represented in the main part of the figure are appropriate for the $Pm\bar{3}m$ cubic structure. Indeed, small amounts of peak splitting appropriate to the departure of the cell dimensions from cubic are present. Not all of these peak splittings are captured in the figure owing to the small amount of splitting compared to the sampling interval in the *x* axis. The inset expands the region around the (1 1 1) diffraction peak. Here diffraction peaks in the *Pbnm* setting are located. These super-lattice diffraction peaks disappear in the cubic structure and are related to the tilting of the octahedra. The calculated peaks are present for the structures studied here, but they are quite small. There exists a possibility that longer time calculations may find these peaks becoming even smaller. They are likely to be very difficult to detect experimentally, yet

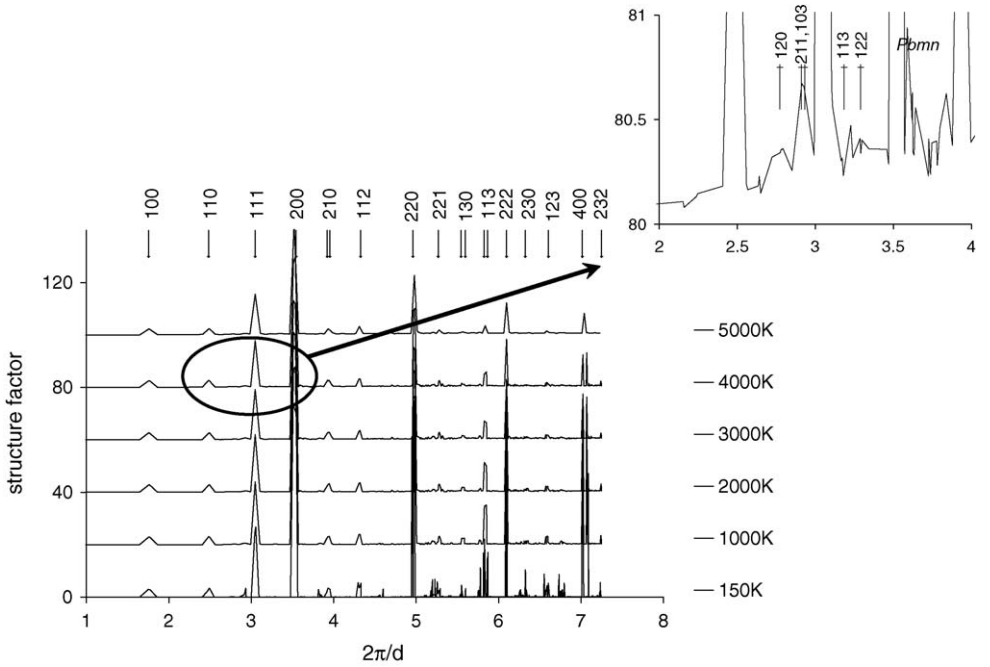

Fig. 10. Structure factor as a function of wave number for calculated $CaSiO_3$ perovskite structures at several temperatures. Structure factors are calculated for each frame separated 1 fs in time including 1000 frames. Hydrostatic conditions for the equilibrated structure with a cell volume of 45.53 $Å^3$ define the model. The 150 K cell is orthorhombic; the 1000–4000 K cells are tetragonal; the 5000 K cell is cubic. Peak indices in the main figure are referenced to the aristotype, cubic, $Pm\bar{3}m$ space group. The inset figure is an enlargement of the 4000 K diffraction pattern with peak indices referenced to the *Pbnm* space group indicating supper-lattice reflections. This section is representative of the other diffraction patterns.

they betray the fact of the departure of the atom positions from those of the cubic symmetry. The low intensity of these super-lattice reflections explain why Shim et al. (2002) only see the splitting of the cubic peaks and no clear evidence of super-lattice reflections. Indeed, their results (such as the *c*/*a* ratio) are in excellent agreement with this study.

6. Conclusions

An AIMD calculation on $CaSiO_3$ perovskite at high pressure and high temperature has allowed us to investigate the dynamics of the phase stability of $CaSiO_3$ perovskite by analyzing the equilibrated stresses and atom positions as a function of time at the femto-second time scale. We find that the octahedral tilts remain significant with little variation in magnitude to the highest temperatures, where the structure may be either tetragonal or cubic on some time scales. This observation goes counter to the model in which the phase transitions are accomplished through the vanishing of the octahedral tilts. Thermal expansion is accomplished purely by Si–O bond length increases. Similarly, compression is accomplished by Si–O bond shortening. The distortion of the octahedra accounts for the tetragonal distortion of the cubic phase at high temperature. Calculated X-ray diffraction patterns indicate that the tetragonal distortion is mostly observed through splitting of the cubic diffraction peaks while super-lattice reflections of orthorhombic symmetry are present with small intensities.

A stable tetragonal structure for $CaSiO_3$ perovskite in the Earth's lower mantle can be important in determining Q of the region. $CaSiO_3$ perovskite can be the source of acoustic absorption due to its small ferroelatic strain, for which domain-wall motion induced by acoustic stress absorbs acoustic energy (Harrison et al., 2003). This issue awaits further experimental exploration.

Acknowledgements

This work is support by NERC (Grant Nos. NER/T/S/2001/00855; NER/O/S/2001/01227), and computer facilities provided by NERC at University College London, and the High Performance Computing Facilities of the University of Manchester (CSAR) and the Daresbury Laboratory (HPCx). DJW acknowledges the Leverhulme Trust for support through the visiting Professor program. DJW and LL acknowledge NSF

EAR-9909266, EAR0135551, EAR0135550. MPI publication 360. R. Wentzcovitch acknowlege NSF EAR-0135533 and ITR-0428774 (VLab).

References

Adams, D., 2004. Molecular Dynamics Simulations of Cubic $CaSiO_3$ perovskite: an Ab Initio Study. In: Proceedings of the CECAM Workshop on "First-Principles Simulations: Perspectives and Challenges in Mineral Sciences", Berichte aus Arbeitskreisen der DGK, Nr. 14, German Crystallographic Society, pp. 79–82.

Akber-Knutson, S., Bukowinski, M.S.T., Matas, J., 2002. On the structure and compressibility of $CaSiO_3$ perovskte. Geophys. Res. Lett. 29 (3), 1034.

Alfè, D., 1999. Ab-initio molecular dynamics, a simple algorithm for charge extrapolation. Comput. Phys. Commun. 118, 31–33.

Allen, M.P., Tildesley, D.J., 1997. Computer Simulation of Liquids. Oxford University Press, New York, NY, USA, 408 pp.

Blöchl, P.E., 1994. Projector augmented-wave method. Phys. Rev. B 50, 17953–17979.

Caracas, R., Wentzcovitch, R.M., 2005. Equation of state and stability of $CaSiO_3$ under pressure. Geophys. Res. Lett. 32 (4), L06303.

Carpenter, M.A., Redfern, S.A.T.e., Carpenter, M.A.e., 2000. Strain and elasticity at structural phase transitions in minerals. Transformation processes in minerals. Rev. Mineral. Geochem. 39, 35–64.

Glazer, A.M., 1972. The classification of tilted octahedra in perovskites. Acta Crystallogr. B 28, 3384.

Glazer, A.M., 1975. Simple ways of determining perovskite strucutres. Acta Crystallogr. A 31, 756.

Harrison, R.J., Redfern, S.A.T., Street, J., 2003. The effect of transformation twins on the seismic-frequency mechanical properties of polycrystalline $Ca_{1-x}Sr_xTiO_3$ perovskite. Am. Mineral. 88, 574–582.

Jung, D.Y., Oganov, A.R., 2005. Ab initio study of the high-pressure behavior of $CaSiO_3$ perovskite. Phys. Chem. Miner. 32 (N2), 146–153.

Karki, B.B., Wentzcovitch, R.M., de Gironcoli, S., Baroni, S., 2001. First principles thermoelasticity of $MgSiO_3$-perovskite; consequences for the inferred properties of the lower mantle. Geophys. Res. Lett. 28 (14), 2699–2702.

Kresse, G., Furthmüller, J., 1996a. Efficiency of ab-initio total energy calculations for metals and semiconductors using a plane-wave basis set. Comput. Mat. Sci. 6, 15–50.

Kresse, G., Furthmüller, J., 1996b. Efficient iterative schemes for ab initio total-energy calculations using a plane-wave basis set. Phys. Rev. B 54, 11169.

Kresse, G., Joubert, D., 1999. From ultrasoft pseudopotentials to the projector augmented-wave method. Phys. Rev. B 59, 1758–1775.

Li, L., Brodholt, J.P., Stackhouse, S., Weidner, D.J., Alfredsson, M., Price, G.D., 2005. Elasticity of (Mg, Fe) (Si, Al)O_3-perovskite at high pressure. Earth Planet. Sci. Lett. 240 (2), 529–536.

Magyari-Kope, B., Vitos, L., Grimavall, G., Johansson, B., Kollar, J., 2002. Low-temperature crystal strucutre of $CaSiO_3$ perovskite: an ab initio total energy study. Phys. Rev. B 65, 193107.

Oganov, A.R., Brodholt, J.P., Price, G.D., 2001. Ab initio elasticity and thermal equation of state of $MgSiO_3$ perovskite. Earth Planet. Sci. Lett. 184 (3–4), 555–560.

Ono, S., Ohishi, Y., Mibe, K., 2004. Phase transition of Ca-perovskite and stability of Al-bearing Mg-perovskite in the lower mantle. Am. Mineral. 89, 1480–1485.

Perdew, J.P., et al., 1992. Atoms, molecules, solids, and surfaces: applications of the generalized gradient approximation for exchange and correlation. Phys. Rev. B 46, 6671–6687.

Shim, S.-H., Duffy, T.S., Shen, G., 2001. Stability and structure of $MgSiO_3$ perovskite to 2300-kilometer depth in Earth's mantle. Science 293 (5539), 2437–2440.

Shim, S.-H., Jeanloz, R., Duffy, T.S., 2002. Tetragonal structure of $CaSiO_3$ perovskite above 20 GPa. Geophys. Res. Lett. 29 (24), 2166.

Stixrude, L., Cohen, R.E., 1993. Stability of orthorhombic $MgSiO_3$ perovskite in the Earth's lower mantle. Nature (London) 364 (6438), 613–616.

Wang, Y., Perdew, J.P., 1991. Correlation hole of the spin-polarized electron-gas, with exact small-wave-vector and high density scaling. Phys. Rev. B 44, 13298–13307.

Wentzcovitch, R.M., Ross, N.L., Price, G.D., 1995. Ab initio study of $MgSiO_3$ and $CaSiO_3$ perovskites at lower-mantle pressures. Phys. Earth Planet. In. 90 (1–2), 101–112.

Wolf, G.H., Jeanloz, R., 1985. Lattice dynamics and structural distortions of $CaSiO_3$ and $MgSiO_3$ perovskites. Geophys. Res. Lett. 12 (7), 413–416.